J Sol-Gel Sci Technol (2011) 58:360–365
DOI 10.1007/s10971-011-2401-3

ORIGINAL PAPER

Preparation, characterization and photocatalytic properties of TiO_2 nanostructured spheres synthesized by the Sol–Gel method modified with ethylene glycol

K. Del Ángel-Sánchez · O. Vázquez-Cuchillo · M. Salazar-Villanueva · J. F. Sánchez-Ramírez · A. Cruz-López · A. Aguilar-Elguezabal

Received: 31 May 2010 / Accepted: 6 January 2011 / Published online: 22 January 2011

Abstract Monodispersed nanostructured TiO_2 spheres were obtained by the Sol–Gel method modified with ethylene glycol. The sample morphology and surface textural properties were characterized by X-ray diffraction (XRD), N_2-physisorption, scanning electron microscopy (SEM), transmission electron microscopy (TEM), thermogravimetric analysis (TGA) and diffuse reflectance spectroscopy (DRS). The SEM image showed spheres with sizes ranging from 600 to 700 nm. In addition, HRTEM micrographs reveal hexagonal grains slightly elongated (20 nm). The powders present a BET surface area of 116 $m^2\ g^{-1}$. Samples without thermal treatment and those treated at 400 °C both showed characteristic reflections of the anatase phase. The photocatalytic activity of the prepared TiO_2 spheres was determined by degradation of 2,4-dichlorophenoxyacetic acid (2,4-D) in aqueous solution. Kinetics parameters have displayed than the nanostructured material present a reaction half-life time of 30 min and it was two times faster than commercial TiO_2 (P25).

Keywords TiO_2 spheres · Photocatalysis · 2,4-Dichlorophenoxyacetic acid · Sol–Gel

K. Del Ángel-Sánchez · A. Aguilar-Elguezabal
Centro de Investigación en Materiales Avanzados (CIMAV), Ave. Miguel de Cervantes 120, Complejo Industrial Chihuahua, 31109 Chihuahua, Chihuahua, México

O. Vázquez-Cuchillo · A. Cruz-López (✉)
Facultad de Ingeniería Civil, Universidad Autónoma de Nuevo León, Av. Universidad y Av. Fidel Velázquez S/N, Cd. Universitaria, 66451 San Nicolás de los Garza, Nuevo León, México
e-mail: cruz_lopeza@yahoo.com.mx

M. Salazar-Villanueva
Facultad de Ingeniería, Universidad Autónoma de Puebla, Apartado Postal J-39, 72570 Puebla, México

J. F. Sánchez-Ramírez
Unidad Profesional Interdisciplinaria en Ingeniería y Tecnologías Avanzadas del Instituto Politécnico Nacional, Av. Instituto Politécnico Nacional, 2580. Barrio Laguna Ticomán, 07340 México, México

1 Introduction

In recent years, materials at the nanometric level have attracted the attention of theoretical and experimental researchers [1–5], with the aim of finding new applications for these materials, such as hydrogen storage [6], dielectric applications [7], biosensing [8] and gas sensing [9], among others [10–13]. In particular, nanosized TiO_2 has proven to be the most popular photocatalyst for the elimination of environmental pollutants [14–16], along with other applications, including anodes for batteries [17], hydrogen production [18] and self-cleaning films [19]. Designing a TiO_2 nanostructure with large surface area, high crystallinity and controlled shape and pore structure is a crucial subject for realization of these applications. Many studies on TiO_2 have focused on the synthesis of uniform spheres with control of their particle sizes at the nanometric scale using conventional methods, such as the hydrothermal method [20], templating method [21], sol–gel method [22], and micelle and inverse micelle methods [23, 24]. However, not all of these procedures have led to positive results. The applications of titania strongly depend on its crystalline structure, morphology, particle size and acid–base properties. More recent works have attempted to obtain nanostructured particles with highly homogeneous morphologies [25–28] to improve their catalytic performance and electrochemical properties [29]. In this paper,

monodispersed nanostructured spherical TiO_2 particles were prepared by a simple and reproducible method. The structural, morphological, optical and photocatalytic properties of the samples were investigated using scanning electron microcopy (SEM), thermogravimetric analysis (TGA), X-ray diffraction (XRD), transmission electronic microscopy (HRTEM), optical absorption spectroscopy in the Uv–Vis range and nitrogen adsorption isotherms. The samples showed high photocatalytic activity and were evaluated in the decomposition of the herbicide 2,4-dichlorophenoxyacetic acid (2,4-D). The synthesized particles demonstrated a reaction half-life almost two times faster than TiO_2 (P25).

2 Experimental

2.1 TiO_2 spheres preparation

All chemicals were of analytical grade and were used without further purification. Commercially available TiO_2 Degussa P-25 (Nippon Aerosil Co., Ltd.) was selected for comparative studies. To obtain the nanostructured spheres of TiO_2, we used a hydrolysis process. 0.56 mL of tetrabutyl orthotitanate (TBOT, Fluka, 97%) was mixed with 50 mL of ethylene glycol (EG, Fisher) in an inert environment (N_2) to avoid the effect of humidity in the hydrolysis reaction. This solution of titanium precursor (solution "A") was magnetically stirred for approximately 20 h at room temperature. This step has been reported to be an important modification of the reaction protocol because the glycol radicals become electronegative sites, thereby attracting titanium ions, leading to formation of the spheres [30]. A possible pathway of the chemical reaction of solution A is shown in Eq. 1. Further, 98 mL of acetone were mixed with 2 mL of distilled water (solution "B"). Thus, nanoparticles of TiO_2 were obtained by mixing solutions A and B. This process is explained in Eq. 2. The role played by the acetone is not clear, but it likely controls the rate of hydrolysis of the glycolate precursor [25, 28]. The TiO_2 spheres were washed and redispersed in an ultrasonic bath in a solution of ethanol/water (1:1 v/v). This process was repeated two times, followed by separation by centrifugation. To remove excess ethylene glycol from the particle surfaces, they were dried at 80 °C for 16 h, followed by calcination at 400 °C in air for 4 h.

$$\mathrm{Ti(OBu)_4 + 2\,OHCH_2CH_2OH \rightarrow Ti(OCH_2CH_2O)_2 + 4\,BuOH} \quad (1)$$

$$\mathrm{Ti(OCH_2CH_2O)_2 + 4\,H_2O \rightarrow Ti(OH)_4 + 2\,OHCH_2CH_2OH} \quad (2)$$

2.2 Characterization

The structural properties were determined by X-ray diffraction using a Bruker D8 Advance at a scanning rate of 0.02° per second for 2θ in the range of 20–70°. The grain size was calculated from XRD results according to the Scherrer's equation [31].

$$D = (0.9\lambda).(\beta \cos\theta) \quad (3)$$

where D is the average grain size in nanometer, λ is the radiation wavelength (0.154 nm), β is the corrected half-width at half-maximum (FWHM), and θ is the diffraction peak angle.

The physical adsorption of N_2 at 196 °C was performed using a Quantachrome 3B automatic instrument to measure specific surface area. Before nitrogen adsorption, the catalyst was out-gassed at 350 °C for 12 h to remove adsorbed impurities. The BET method was applied to determine the specific surface area. Thermo gravimetric analysis (TGA) of fresh samples were performed in a Q600 TA-Instruments apparatus at a heating rate of 10 °C min^{-1} under a flow of nitrogen gas. The reflectance spectra of the solids were obtained in air and at room temperature with a UV–Vis Perkin Elmer spectrophotometer lambda 35. The band gap was calculated by measurement of the diffuse reflectance of the TiO_2 using the Kubelka–Munk reflectance transfer model [32]. The morphologies of the samples were analyzed by scanning electron microscopy (SEM, JEOL 6490 LV microscope). For SEM observation, a drop of solution was spread on a carbon-coated copper microgrid and covered with a thin film of gold. TEM analysis was recorded with a JEM-2200FS microscope operating a 200 kV with a HAADF detector.

2.3 Photocatalytic decomposition of 2,4-D

Sample photodegradation following calcination at 400 °C was determined by monitoring 2,4-dichlorophenoxyacetic acid (2,4-D) decomposition at room temperature under UV light irradiation. In a closed box, a stirred solution was irradiated with a Pen-Ray model 90-0012-01 lamp, which emits at $\lambda = 254$ nm with an intensity of 2,000 μW cm^{-2}. The quartz lamp was immersed in a refrigerated vessel containing the reactant solution (100 mL with 40 ppm of 2,4-dichlorophenoxyacetic acid and 100 mg of photocatalyst). To achieve saturation of dissolved oxygen and assure adsorption of 2,4-D on the semiconductor, a flux of dry air was bubbled for 60 min (1 mL s^{-1}) before the light source was turned on. The concentration of the 2,4-dichlorophenoxyacetic acid was calculated from the adsorption band at 229 nm as a function of irradiation time by observation with a Perkin Elmer lambda 35 UV–Vis spectrophotometer.

3 Results and discussion

3.1 Catalyst characterization

The shape and size of the prepared TiO_2 particles treated at 400 °C were evaluated by scanning electron microscopy (see Fig. 1). From the images, the particles had a shape close to spherical and a smooth surface. Figure 1b shows that the size distribution was a Gaussian fit, where the average diameter calculated was around 0.74 μm. The value of the standard deviation suggested that the obtained nanospheres were homogenous. The diameter of the microspheres showed a decrease upon heat treatment that was likely due to the loss of solvent or organic matter during the calcination process, as indicated by the thermogravimetric analysis (TGA) results. Figure 2 shows the TGA curve, where 100 °C; a weight loss of almost 7% was due to the removal of water/alcohol still present in the sample. The second loss at temperatures higher than 200 °C was 13% of the whole mass was associated with evaporation of the glycolated species formed between the titanium precursor and ethylene glycol [25, 28]. The last significant change, at approximately 335 °C, was a weight loss close to 11% to due to dehydroxylation upon thermal treatment, associated with the conversion of $Ti(OH)_4$ into TiO_2 as showed in Eq. 4.

$$Ti(OH)_4 \rightarrow TiO_2 + 2H_2O \quad (4)$$

It is well known that 3 polymorphs of TiO_2 exist and every one of them favor by controlling synthesis parameters [33] Pal et al. [28] reported the synthesis of fully amorphous TiO_2 spheres at 100, and 400 °C the presence of anatase phase. On the other hand several authors have reported the presence of rutile phase after 400 °C [34, 35]. In our case, the diffraction peaks of the as-synthesized product are shown in Fig. 3a. The peak reflections for the (*101*), (*004*), (*200*), (*105*), (*211*), (*213*) and (*116*) directions were very wide, which is a feature of semi-crystalline anatase (JCPDS File No. 21-1272). The sample annealed at 400 °C in air during 4 h, revealed more intense and narrow reflections (see Fig. 3b). This proved that an increase in crystallinity had occurred after heat treatment. The signals were indexed according to the body-centred teragonal cell for TiO_2, space group l41/amd, a = b = 3.7852 Å, c = 9.5139 Å. In Fig. 3c, the pattern of diffraction is shown for the TiO_2 (P25) sample at 400 °C only reference, which had similar features to the anatase phase (3a and 3b), although one reflection was found at 28°, which corresponded to the (*100*) crystalline plane of the rutile phase.

The average size of the anatase crystallites in the synthesized samples was estimated using the Scherrer equation (Eq. 3 in Sect. 2), and the line of the XRD peak at around 26.1°, which is associated with the (*101*) crystallographic plane. The calculated crystallite size was 20 nm in diameter. Combined with the TEM observations (see Fig. 4a), we concluded that the sample synthesized by our route and treated at 400 °C had a spherical shape and crystallinity of TiO_2 particles. Additionally, each one of these spheres appeared to be constructed from particles with a size close to 20 nm in diameter. The corresponding TEM images revealed the presence of uniformly sized mesopores with a disordered structure. Nowadays, this structure is different from the spherical structures reported by other researchers [33, 36].

In order to explore the crystal structure of TiO_2 in more detail, the HRTEM analysis for the calcined sample was performed. Figure 4b shows the HRTEM micrographs, there can be seen hexagonal grains slightly elongated (20 nm). The analysis has proved the nature of anatase

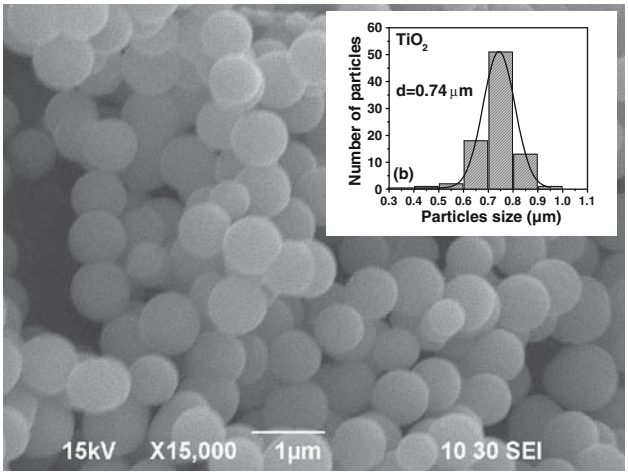

Fig. 1 SEM images of TiO_2 particles after annealing at 400 °C and their size distribution (*insert*)

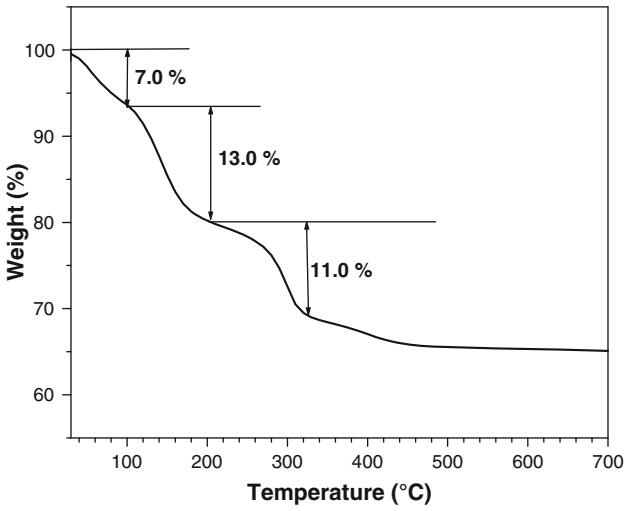

Fig. 2 Thermogravimetry analysis (TGA) of the prepared TiO_2 spheres

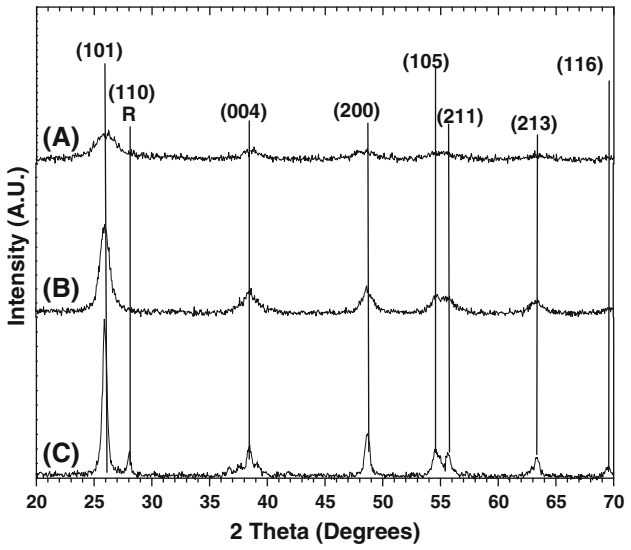

Fig. 3 XRD patterns of TiO_2 spheres (*a*) as-grown, (*b*) annealed at 400 °C and (*c*) TiO_2 (P25) annealed at 400 °C

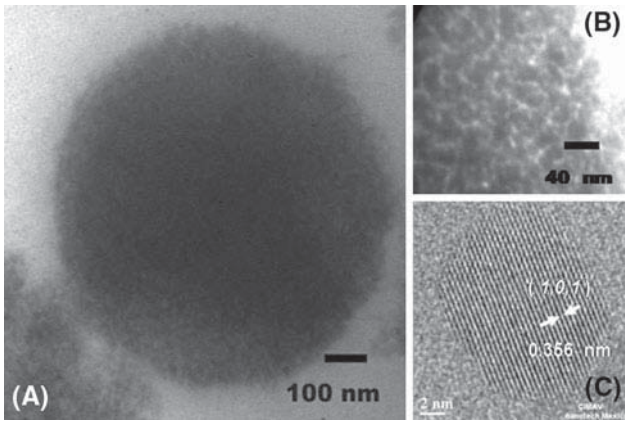

Fig. 4 TEM and HRTEM images of TiO_2 spheres after annealed at 400 °C

crystal with a d-spacing 0.35 nm. This d-spacing value is assigned to the lattice spacing of the (1 0 1) planes of the anatase phase (see Fig. 4c). Several authors agree on the importance of obtaining a control on the morphology of the synthesized materials at the nanoscale, to increase the photoactivity of the materials [29, 37, 38], Kudo [39] explains the small particle size is beneficial in terms of increasing the probability of the reaction of photogenerated electrons and holes in photocatalyst reactions.

Determination of the band gap energy was essential for identification of changes in the electronic structure of the titania spheres, which depends on the structural properties. Figure 5 shows the band gap energy was obtained using a reflectance technique by applying the Kubelka–Munk theory and was estimated from the intercept of the tangents to the plots to be 3.28 and 3.29 eV for the TiO_2 spheres and TiO_2 (P25), respectively characteristic of anatase phase [39, 40].

The measure of the specific area of the nanoparticles was obtained using the BET method with the adsorption–desorption of nitrogen at −196 °C. These samples were previously heat treated at 400 °C. Figure 6 shows a traditional isotherm of TiO_2 spheres with a surface area of 116 $m^2\ g^{-1}$. This profile could be classified as type IV, which is characteristic of mesoporous materials. Figure 6b shows the pore-size distribution plots calculated using the BJH equation from the desorption isotherm. The pore size distribution measurement indicated that the TiO_2 spheres had a pronounced mesoporosity with a narrow pore-size distribution of around 3 nm in diameter, along with a small portion of larger pores (<100 nm). This pore size is produced by the slow nucleation of TiO_2 particles and is the main reason for the obtained surface area, it has been reported by other authors to show a direct relationship between nucleation rate and the area obtained [14, 15].

3.2 Catalyst evaluation

The enhancement in photocatalytic performance in oxides semiconductors for the degradation of organic compounds can be explained by the higher surface area with mesoporous structure, reduction in the crystallite size, defects and band gap. In this respect, the morphological structure may also contribute to some extent to the superior activity of the present TiO_2 spheres structures. The spheres synthesized in this work were tested in the photocatalytic degradation of 2,4-D under ultraviolet light and compared with P25. The results are shown in Fig. 7. The photolysis reaction without catalyst showed a degradation of about

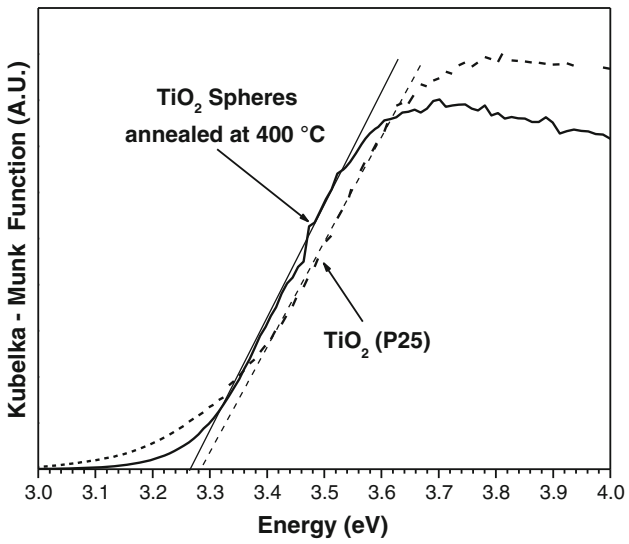

Fig. 5 Kubelka-Munk-transformed diffuse reflectance spectra (DRS) of the samples

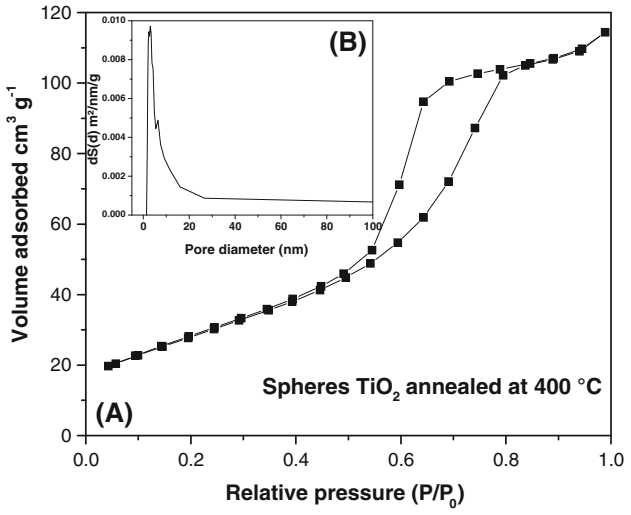

Fig. 6 N_2 adsorption–desorption isotherms and pore size distributions (*insert*) of the TiO_2 spheres calcined at 400 °C

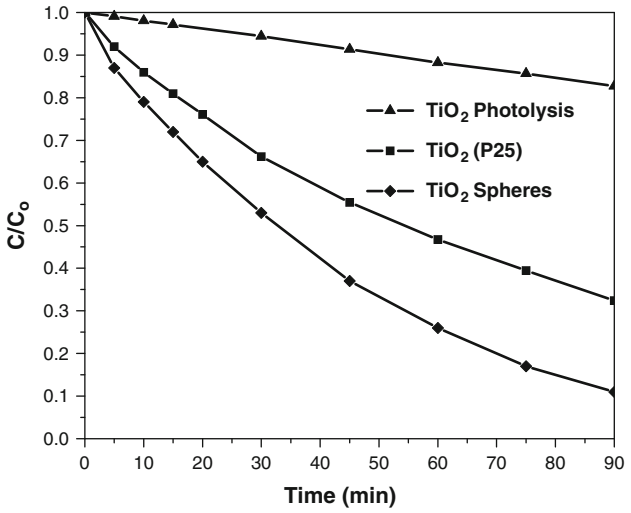

Fig. 7 Comparison of the photocatalytic activities of the catalyst annealed at 400 °C in the degradation of 2,4-dichlorophenoxyacetic acid under exposure to UV light

18% after 90 min of exposure to ultraviolet radiation. Conversely, the spheres of TiO_2 showed 89% degradation of 2,4-D after 80 min. The kinetic parameters of the photocatalytic reaction, k and $t_{1/2}$, were calculated following a first order reaction model: $\ln(Co/C) = kt$. Calculations were done using the data shown in Fig. 8. The linear behavior of each curve indicated that a first order reaction was taking place during 2,4-D degradation. According to the kinetic parameters, the best photocatalytic activity was observed with TiO_2 spheres after treatment at 400 °C, which showed a half-life time of 30 min compared with 54 min of TiO_2 (P25). The high activity of the synthesized spheres is attributed to the morphology presented which is composed of anatase crystals in the form of elongated

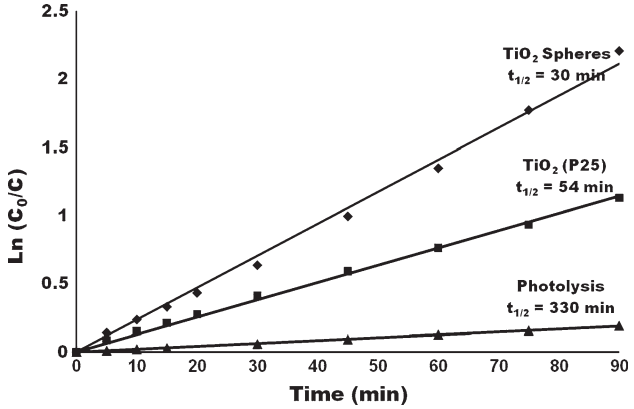

Fig. 8 Kinetic order of the degradation of 2,4-D in the presence of TiO_2 and thermally treated at 400 °C

hexagons, which probably would delay the electro hole recombination accelerating the degradation of organic contaminate in combination with the surface areas, 116 and 54 $m^2\ g^{-1}$ for the TiO_2 spheres and TiO_2 (P25), respectively. Several authors have shown that the degradation of 2,4-D is strongly influenced by the surface area of TiO_2 [14, 15], which is enhanced by the presence of dopants that reduce the value of the band gap energy of pure semiconductor decreasing the electron–hole recombination [41, 42]. However, it has shown that materials with highly homogeneous morphology have a high activity attributed to the presence of a greater number of vertices on morphologies [37–39].

4 Conclusions

This report describes the preparation of TiO_2 semi-crystalline with spherical morphology, high surface area and good photocatalytic properties in the decomposition of the herbicide 2,4-dichlorophenoxyacetic acid.

The reaction half-life results displayed that spheres of TiO_2 ($t_{1/2} = 30$ min) were two times more reactive than TiO_2 (P25) ($t_{1/2} = 54$ min). The high activity of spheres is due mainly to the synergetic phenomenon between the nanostructure properties and the geometry of crystals on the surface of the spheres of TiO_2.

Acknowledgments We wish to thank to PROMEP-SEP (103.5/08/3125 and 103.5/08/5466), CONACYT (089620, 081437), PAICYT UANL-2009 and the UANL foundation. K. Del Ángel-Sanchez wishes to express her gratitude to the CONACYT for her PhD grant.

References

1. Gutierrez Fuentes R, Pescador Rojas JA, Jiménez-Pérez JL, Sanchez Ramirez JF, Cruz-Orea A, Mendoza-Alvarez GJ (2008) Appl Surf Sci 255:781

2. Salazar Villanueva M, Romero AH, Bautista Hernández A (2009) Nanotech 20:465709
3. Cruz-López A, Vázquez-Cuchillo O, Juárez Ramírez I, Bautista-Carrillo LM, Zarazua-Morin E (2008) J Ceramic Process Res 9:474
4. Burda C, Chen X, Narayanan R, El-Sayed MA (2005) Chem Rev 105:1025
5. Yin Y, Alivisatos AP (2005) Nature 437:664
6. Torres-Martínez LM, Gómez R, Vázquez-Cuchillo O, Juárez-Ramírez I, Cruz-López A, Alejandre Sandoval FJ (2010) Catal Commun 12:268–271. doi:10.1016/j.catcom.2010.09.032
7. Tchoul MN, Fillery SP, Koerner H, Drummy LF, Oyerokun FT, Mirau PA, Durstock MF, Vaia RA (2010) Chem. Mater 22:1749
8. Jungbase K, Jay WG (2003) Nano Lett 3:1219
9. Zhang JT, Liu JF, Peng Q, Wang X, Li YD (2006) Chem Mater 18:867
10. Deng Z, Yan H, Liu Y (2009) J Am Chem Soc 131:17744
11. Smith AM, Nie S (2010) Acc Chem Res 43:190
12. Liane MR, Li SF, Frank HQ, Rosenzweig Z (2005) Langmuir 21:4277
13. Deng H, Li X, Peng Q, Wang X, Chen J, Li Y (2005) Angew Chem Int Ed 44:2782
14. Vázquez-Cuchillo O, Cruz-López A, Bautista-Carrillo LM, Bautista-Hernández A, Torres Martínez LM, Lee SW (2010) Res Chem Intermed 36:103
15. Galindo F, Gómez R, Aguilar M (2008) J Mol Catal A Chem 281:119
16. Murugan K, Rao TN, Gandhi AS, Murty BS (2009) J Catal Commun 11:518
17. Wang J, Bai Y, Wu M, Yin J, Zhang WF (2009) J Power Sources 191:614
18. Chattopadhyay J, Kim HR, Moon SB, Pak D (2008) Int J Hydrogen Energy 33:3270
19. Wang H, Hu Y, Zhang L, Li C (2010) Ind Eng Chem Res 49:3654
20. Titirici MM, Antonietti M, Thomas A (2006) Chem Mater 18:3808
21. Qian HS, Lin GF, Zhang YX, Gunawan P, Xu R (2007) Nanotech 18:355602
22. Zhang YX, Li GH, Wu YC, Xie T (2005) Mater Res Bull 40:1993
23. Lim KT, Hwang HS, Ryo W, Johnston KP (2004) Langmuir 20:2466
24. Kim KD, Kim SH, Kim HT (2005) Colloids Surf A 254:99
25. Xuchuan J, Thurston H, Younan X (2003) Adv Mater 15:1205
26. Hyung Kyun Y, Gi-Ra Y, Se-Heon K, Seung-Man Y (2007) Lasers and electro-optics—pacific rim, Conference on. doi: 10.1109/CLEOPR.2007.4391348
27. Ao Y, Xu J, Fu D, Yuan Ch (2009) Micropo Mesopo Mater 118:382
28. Pal M, García-Serrano J, Santiago P, Pal U (2007) J Phys Chem C 111:96
29. Xiaofang L, Kangle L, Kejian D, Junfeng T, Rong S, Jie S, Chen L (2009) Mater Sci Eng B 158:40
30. Hua GY, Hua CZ (2004) J Phys Chem B 108:3492
31. Cullity BD (1978) Elements of X-ray diffraction. Wesley, Reading
32. Escobedo Morales A, Sánchez Mora E, Pal U (2007) Rev Mex Fis S 53:18
33. Carp O, Huisman CL, Reller A (2004) Prog Solid State Chem 177:32–33
34. Xuchuan J, Thurston H, Younan X (2003) Adv Mater 15(14):1205–1209
35. Oskam G, Nellore A, Lee PR, Searson PC (2003) J Physics Chem B 107:1734–1738
36. Kim YJ, Yong S, Chai X, Lee W (2007) Langmuir 23(19):9567–9571
37. Li D, Haneda H (2003) Chemosphere 51:129–137
38. Liao DL, Liao BQ (2007) J Photochem Photobiol A Chem 187:363–369
39. Kudo A, Meseke Y (2009) Chem Soc Rev 38:253–278
40. Dong F, Zhao W, Wu Z, Guo S (2009) J Hazard Mater 162:763–770